Applied Surface Science 439 (2018) 623–631

Contents lists available at ScienceDirect

Applied Surface Science

journal homepage: www.elsevier.com/locate/apsusc

Full Length Article

An investigation into the mechanism for enhanced mechanical properties in friction stir welded AA2024-T3 joints coated with cold spraying

N. Li [a,b], W.Y. Li [a,*], X.W. Yang [a], Y. Feng [a], A. Vairis [a,c]

[a] State Key Laboratory of Solidification Processing, Shaanxi Key Laboratory of Friction Welding Technologies, Northwestern Polytechnical University, Xi'an 710072, PR China
[b] Shaanxi Railway Institute, Weinan 714000, Shaanxi Province, PR China
[c] Department of Mechanical Engineering, TEI of Crete, Heraklion, Crete 71004, Greece

ARTICLE INFO

Article history:
Received 19 November 2017
Accepted 5 January 2018
Available online 6 January 2018

Keywords:
Friction stir welding
Cold spraying
Microstructure
Mechanical properties

ABSTRACT

Using cold spraying (CS), a surface layer with a modified microstructure and enhanced mechanical properties was formed on a 3.2 mm thick friction stir welded (FSWed) AA2024-T3 joint. The combined effect of "shot peening effect (SPE)" and "heat flow effect (HFE)" during CS were used to enhance joint mechanical properties. The microstructure evolution of the FSWed AA2024-T3 joints in the surface layer following CS coatings and their effect on mechanical properties were systematically characterized with electron back-scattered diffraction, transmission electron microscopy, differential scanning calorimetry and mechanical tests. Based on these experiments, a grain refinement, finer and more S phases, and improved amount of Guinier-Preston-Bagaryatsky (GPB) zones produced by CS treatments are proposed. The deposition of aluminum coating on the joint, lead to hardness recovery in the stir zone and the development of two low hardness zones as the density of GPB increased. The tensile properties of FSWed AA2024-T3 joints improved with the application of the aluminum coatings. Experiments and analysis of the enhanced mechanical properties mechanism indicate that SPE with a high plastic deformation and HFE with an intensive heat flow are necessary for the production of refined grains and increased numbers of GPB zones.

1. Introduction

Aluminum alloys show high strength, good formability and weight savings which have led them to be used as structural materials in a number of industries, such as aerospace, shipbuilding and automobile [1]. But aluminum alloys are difficult to join with fusion welding techniques because of their poor dentritic solidification microstructure and the development of porosity after welding [2]. Friction stir welding (FSW) is a promising solid-state joining technique that can avoid these solidification defects and lead to improved mechanical properties compared to fusion welding [3,4]. This fact has allowed FSW to be applied widely in the production of high-strength, fatigue and fracture resistance joints with aerospace aluminum alloys, such as the 2XXX and the 7XXX series [5–8].

During FSW, the base material undergoes intense frictional heat which is generated between the tool shoulder and the top of the sheets, while there is a mechanical stirring action by the pin tool rotation [7,9–11]. This intense heat flow and plastic deformation changes during the process, introducing large inhomogeneous areas in the microstructure and varying mechanical properties across the joint [10]. As a consequence, the joint has four typical microstructural zones: the stirred zone (SZ), the thermo-mechanically affected zone (TMAZ), the heat-affected zone (HAZ) and the base material (BM) [11]. Moreover, the rotating tool shoulder damages the covering pure Al layer [12]. As the local microstructure determines mechanical properties and corrosion susceptibility, it is expected that the joint would have lower corrosion resistance and mechanical properties than those of the BM [13,14]. It is therefore important to identify an effective method to improve corrosion resistance and mechanical properties of the joints.

As corrosion performance and mechanical properties of FSWed high-strength aluminum alloys is of prime concern, a number of treatments targeted either at mechanical properties or corrosion resistance of the joints using shot peening (SP) [15,16], post-weld heat treatment (PWHT) [17,18], laser surface melting (LSM) [19–21], micro-arc oxidation (MAO) [22] and other approaches [23,24] have been used. With regards to mechanical properties

* Corresponding author.
E-mail address: liwy@nwpu.edu.cn (W.Y. Li).

https://doi.org/10.1016/j.apsusc.2018.01.049
0169-4332/

improvement, the relationship between microstructure, residual stresses and mechanical properties is available which has the aim of various research efforts to date [15,16,23,24]. The heat treatment (solid solution + aging) method has been widely used to improve tensile strength and microhardness [24], in spite of a number of drawbacks, as it takes a long time, and is limited by the size of the workpiece while it can oxidise the surface and promote grain growth. By comparison, plastic deformation (SP) appears to be more effective, as it can eliminate or modify residual stresses and refine grain size [15,16]. It has been reported that multi-pass laser SP, can change tensile stresses to compressive ones, improve both the tensile strength and fatigue life, but it did not result in improvements in microhardness. The other big challenge of FSW is the low corrosion resistance of the weld [25]. In order to solve this, it has been found that by lowering heat input during welding and PWHT corrosion resistance can be improved to a limited extent, while corrosion problems never do disappear completely due to residual stresses present and the lack of an Al clad layer. Using surface modification techniques (LSM, MAO, etc.), coatings of various thicknesses can provide protection for the joint, while suffering from certain deficiencies. For example, an LSM layer will suffer from partial delamination and element concentration. A MAO layer has a porous surface and requires to be post processed, while reduces the mechanical properties of the joints.

In order to expand the use of FSW it is necessary to identify a technique which both improves mechanical properties and offers corrosion protection to FSWed joints. Cold spraying (CS) is a relatively new solid-state material deposition technique for producing dense coatings, which has the potential for surface protection of FSWed high-strength joints because of corrosion resistance, while offering the important advantage of microstructure modification and improvement of mechanical properties. During CS, the acceleration of particles to high velocities is achieved by expanding a pressurised "hot" gas through a laval nozzle which results in high-velocity impact to the substrate [26]. The hot gas increases particle temperature and increases particle deformation through thermal softening, while heating the substrate, similarly to the "heat flow effect (HFE)" [27,28]. The high velocity impact produces localised large plastic deformation to the substrate, which creates compressive residual stresses in the substrate surface and improves the fatigue performance, similarly to the "shot peening effect (SPE)" [29,30]. Although CS has been studied widely for improving surface corrosion resistance or mechanical properties [31,32], its application to FSWed joints has not been studied at all. In addition, the underlying mechanism for these advantages and the depending factors are not clear.

In this work, the mechanical properties and microstructure evolution of FSWed high-strength aluminum alloy joints which have been CS coated are investigated. In particular, the purpose of this study is: (i) through the design of experiments, to separate the HFE and SPE effects on the CS process; (ii) to examine the microstructure of the FSWed joints under HFE and SPE conditions; and (iii) last but not least, to identify the primary mechanism (i.e. grain size or deformation) and the most important influencing factors (i. e. HFE or SPE) for this process.

2. Experimental study

2.1. FSW experiments

A 3.2 mm thick commercial Al clad AA2024-T3 rolled plate was used as the BM, of length of 200 mm and width of 100 mm. They were butt-welded along the rolling direction with a tool tilt angle of 2.5° (Z-axis) and a plunging depth of 0.2 mm on a commercial FSW machine (FSW-RL31-010, Beijing FSW Technology Co., Ltd., PR China) at a rotation speed of 600 rpm and traveling speed of 200 mm/min. This welding parameter was chosen as the optimum one based on our previous study, as it produces the best mechanical properties [32]. The welding tool had a concave shoulder 10 mm in diameter with a right-hand threaded conical probe of 3.4 mm in diameter and 2.9 mm in length.

2.2. CS experiments

The powders used as feedstock were commercially available gas-atomized aluminum and Al_2O_3 particles, with the latter used as reinforcement in order to avoid blocking of the laval nozzle. A cold-sprayed Al-20 vol.% Al_2O_3 layer was deposited onto the surface of the FSWed AA2024-T3 joint with a CS system developed in the Xi'an Jiaotong University of China. Fig. 1 shows the scanning electron microscope (SEM) micrographs of the free surface of the Al powder and Al_2O_3 particles. The Al powder shows a irregular spherical morphology (Fig. 1a) with the mean particle size being 53 μm. Al_2O_3 particles have an angular morphology (Fig. 1b) with a mean particle size of 70 μm. The nozzle standoff distance from the FSWed joint surface was 30 mm and the traverse speed was set at 60 mm/min. The driving gas was nitrogen at a pressure of 2.8 MPa. Prior to deposition, the flash of joints was removed and no sand-blasting was performed. The CS treatments used in this study are summarized in Table 1.

In order to study the role of coating, HFE and SPE in FSWed joints service, the FSWed joints were coated at 350 °C with and

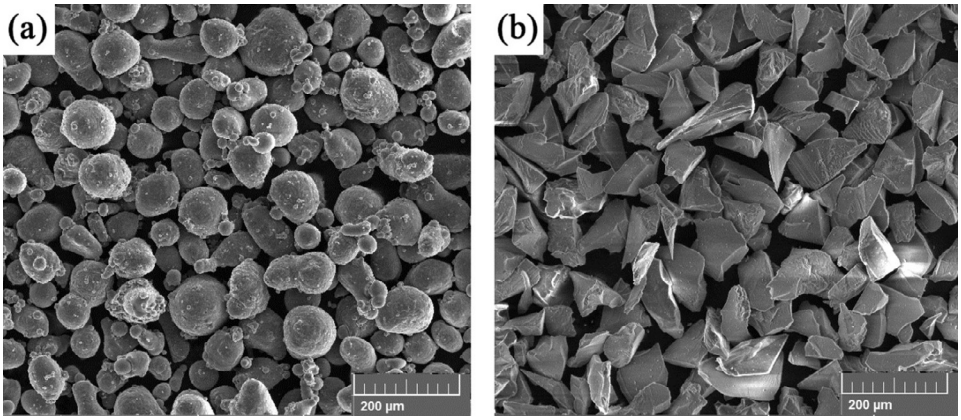

Fig. 1. SEM micrographs of the powders: (a) pure Al powder and (b) Al_2O_3 powder.

Table 1
CS treatments of the FSWed AA2024-T3 joints.

Sample	Gas temperature (°C)	Gas pressure (MPa)	Standoff distance (mm)	Particles	Designation
1	–	–	–	–	As-welded
2	350	2.8	30	Al-20 vol.% Al_2O_3	CSed
3	15	2.8	30	Al-20 vol.% Al_2O_3	Room temperature coated (SPE)
4	350	2.8	30	–	No particles coated (HFE)

without particles, and at 15 °C (room temperature) with particles. Samples coated at room temperature and those coated without any particles are equivalent to the SPE and HFE cases, respectively.

2.3. Characterization

All the FSWed and coated samples to be examined for microstructures were cross-sectioned in a direction perpendicular to the welding direction with an electrical discharge machine. Microstructural characterization and analysis were carried under an optical microscope (OM), SEM, electron back-scattered diffraction (EBSD) and transmission electron microscope (TEM). The specimens for OM observation were ground and polished and then etched with Keller's reagent. The specimens for EBSD were electropolished to produced a strain-free surface. Meanwhile, a differential scanning calorimeter (DSC) was used to identify the precipitation evolution of the joint surface layer at various states during heating at a rate of 10 °C/min in the temperature range of 50–450 °C.

Mechanical properties were evaluated for microhardness and tensile strength. The hardness measurement was conducted along the surface layer of the transverse cross-section of all the joints under a load of 200 g for 15 s. The tests were performed at a distance of 0.3 mm from the top surface of the joints with the interval distance between adjacent measurement points was set at 0.6 mm. In the testing line, there were 70 indentations performed that extended from the centre to as far as 20 mm away on both the retreating side (RS) and the advancing side (AS). Fig. 2 shows the spread of the microhardness tests, together with an indication of various zones across the joint (BM, HAZ, TMAZ and SZ). It was ensured that there was matching between DSC and hardness measurements. Tensile tests were carried out on specimens which were cut in a direction perpendicular to the welding direction. Room temperature tensile tests were carried out at a cross-head speed of 1 mm/min using a computer-controlled testing machine and the tensile properties of each joint reported were the average of three tests.

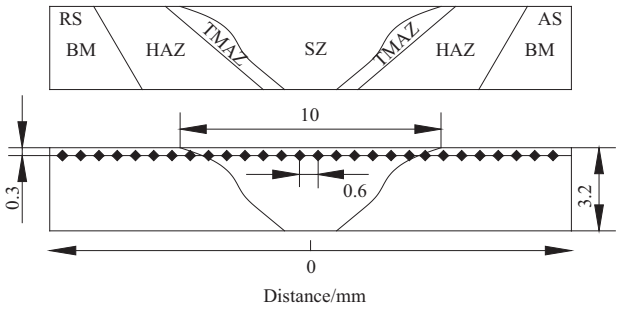

Fig. 2. Spread of microhardness test points.

3. Results and discussion

3.1. Microstructure characteristics

Fig. 3a shows the SEM surface morphologies of the Al-20 vol.% Al_2O_3 coating deposited on the FSWed AA2024-T3 joint. There are few small pores, micro cracks and intact particles on the surface of the coating. As the CS temperature is below that of the melting point of the particles, the particles on the coating surface did not melt. Moreover, without tampping effect of the particles following the those which arrived first at the surface, insufficiently deformed particles identified were consistent. All coatings were strongly attached to the substrate with limited porosity in the surface layer. CSed coatings are known of limited porosity, especially close to the top surface [33,34]. These flaws are dependent on the CS mode of operation [28,34]. Fig. 3b shows a three-dimension image of Al-20 vol.% Al_2O_3 coating on a FSWed A A2024-T3 joint. The image clearly indicates that the surface of coating is rough and its morphology is in good agreement with the SEM micrograph.

Fig. 4 shows the SEM cross sections micrographs of the Al-20 vol.% Al_2O_3 coating. It can be seen that the coating is composed of an Al- Al_2O_3 composite with irregular shaped Al_2O_3 particles scattered through the Al matrix. The coating exhibits a continuous, defect-free interface with the substrate (Fig. 4a). The joint was entirely covered with a coating which had a thickness of about 800 μm. Al particles plastically deform on impact providing improved bonds between all materials present. Metallic oxides,

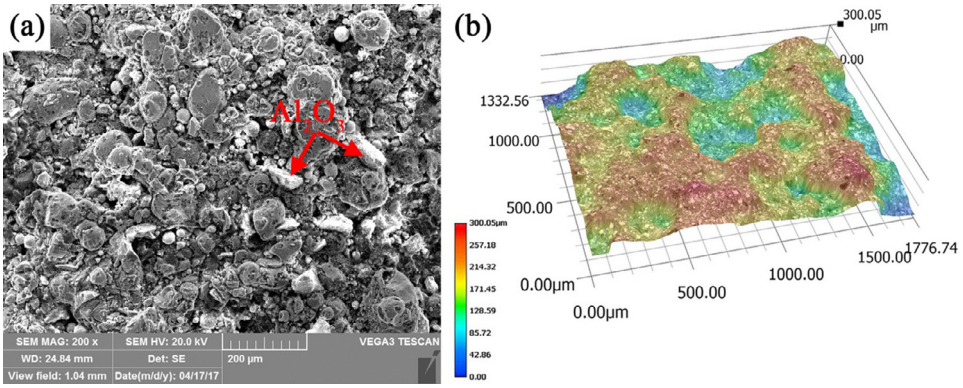

Fig. 3. (a) SEM surface morphologies of the CSed coating and (b) three-dimensional OM images of the coating.

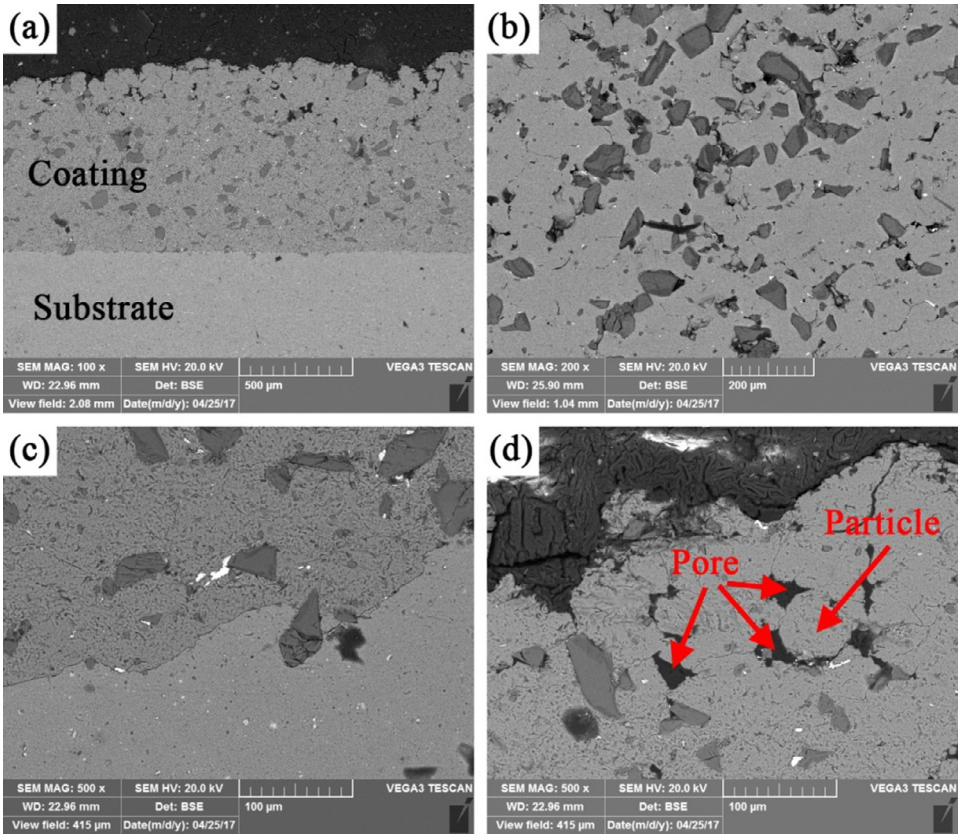

Fig. 4. Cross section images of the coatings: (a) SEM image of the Al-20 vol.% Al_2O_3 coating, SEM image of the coating: (b) middle, (c) inner and (d) top.

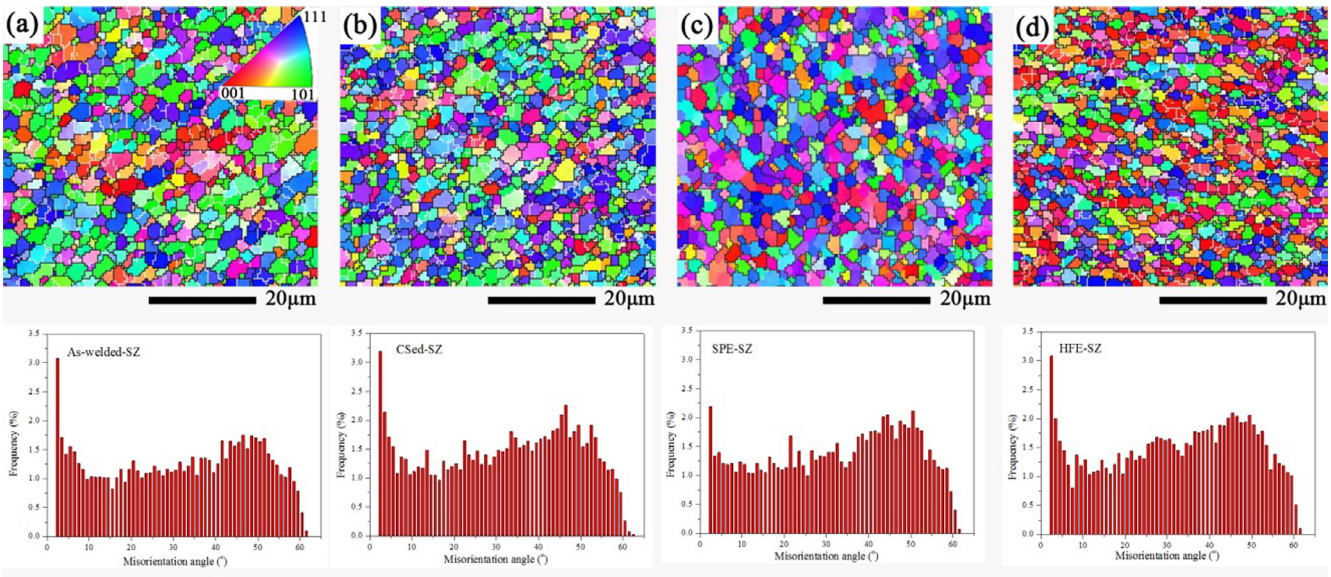

Fig. 5. EBSD maps and misorientation angle distribution in SZs of the joints obtained under (a) as-welded, (b) CSed, (c) SPE and (d) HFE.

cracks and interconnected porosity were not observed at the interface or in the intermediate region of the coating (Fig. 4b). It can be seen that the initial Al_2O_3 particles are larger than the size of Al_2O_3 particles in the coating which are irregular, which may suggest that some of these may have been broken apart from impact. It should be noted that porosity is observed at the top surface of the coating and the top layer is less compact than the bottom layer (Fig. 4c and d). Underneath the porous top surface, a dense region usually occurs in CSed coatings as part of the porosity is closed by tampping of the following incoming particles. These observations are in good agreement with literature where CS coatings have been shown to have limited porosity in the top layer and dense bottom layers [35,36]. In addition, the coatings are not deposited on the joints under SPE and HFE.

Fig. 5 shows the orientation images and misorientation angle distributions for the SZs of the joints for various CS treatments.

All the SZs exhibit a typical uniform fine-equiaxed grain structure and high-angle grain boundaries (HAGBs) (misorientation angle ≥ 15°). The generation of these fine grains is due to intense plastic deformation and frictional heating during FSW, which may lead to dynamic recrystallization and grain refinement when compared to other zones of the FSWed joint [11,37]. It is well established that recrystallization is a nucleation and growth process and the growth is accomplished by the migration of the HAGBs. In this study, the average grain sizes are 2.3 ± 0.07 μm, 1.9 ± 0.07 μm, 2.0 ± 0.07 μm and 1.9 ± 0.11 μm for the SZs produced for the as-welded, CSed, SPE and HFE, cases respectively. Grains following any CS treatment become refined compared to those of the as-welded joints. So grain refinement is the function of CS. It is clear that grain refinement is due to (i) the SPE which causes plastic deformation, refined grains, dislocation cell blocks and shot peening near the surface of the joint [38–41]. In addition, intense plastic deformation can improve the strength of the material by refining the grains [42,43]; (ii) the temperature of the HFE is 200–300 °C, which is the recrystallization temperature of the AA2024 [44]. So HFE causes the top surface of the joint to recrystallize sufficiently. As a consequence, HFE is effective in producing the appropriate grain refinement while reducing the grain size gradient near the surface of the coated joint; (iii) CS combines the two effects of SPE and HFE, but these effects are not simply superposed on each other but work in a cooperating manner. The HAGBs for the SZs produced under as-welded, CSed, SPE and HFE contribute about 57.4%, 67.2%, 65.8% and 70.8% of the total grain boundary length, respectively. Higher HAGBs and refined grains are beneficial as they increase strain hardening. Furthermore, large numbers of HAGBs can hinder and block dislocations more effectively due to high stress concentration, enhancing the strain-hardening capacity and improving the ductility of the joint therefore [45].

Fig. 6a–d displays the brigth-field TEM images in SZs of the top surface layer under different CS treatments. It is clearly known that the SZ is the zone undergone the dynamic recrystallisation, with few dislocations left after welding [7]. In the case of as-welded, number of granule-shaped S phases and few coarse Ω phases are clearly recognized because of the short maintaining time under high temperature during FSW process. However, when the FSWed joints were suffered different CS treatments i.e. CSed, SPE and HFE, the S phase is finer and the fraction is higher. It was well known that the S phase is the main precipitation and the finer S phase in the Al matrix has a pivotal effect in preventing abnormal grain growth and improving the tensile strength by pinning dislocations [9,11,13]. The effect of preventing abnormal grain growth can be expressed by Fig. 5. Furthemore, the size and fraction of the S phase following any CS treament become finer and higher compared to those of the as-welded joints. The SZ of the CSed joint has the finest S phase and highest fraction.

3.2. DSC curves

It is well established that DSC is a reliable and powerful technique to study precipitation and dissolution of second phases in precipitation strengthened Al alloys [46]. Figs. 7a and 6b shows the DSC curves of the SZs and HAZs under various CS treatments,

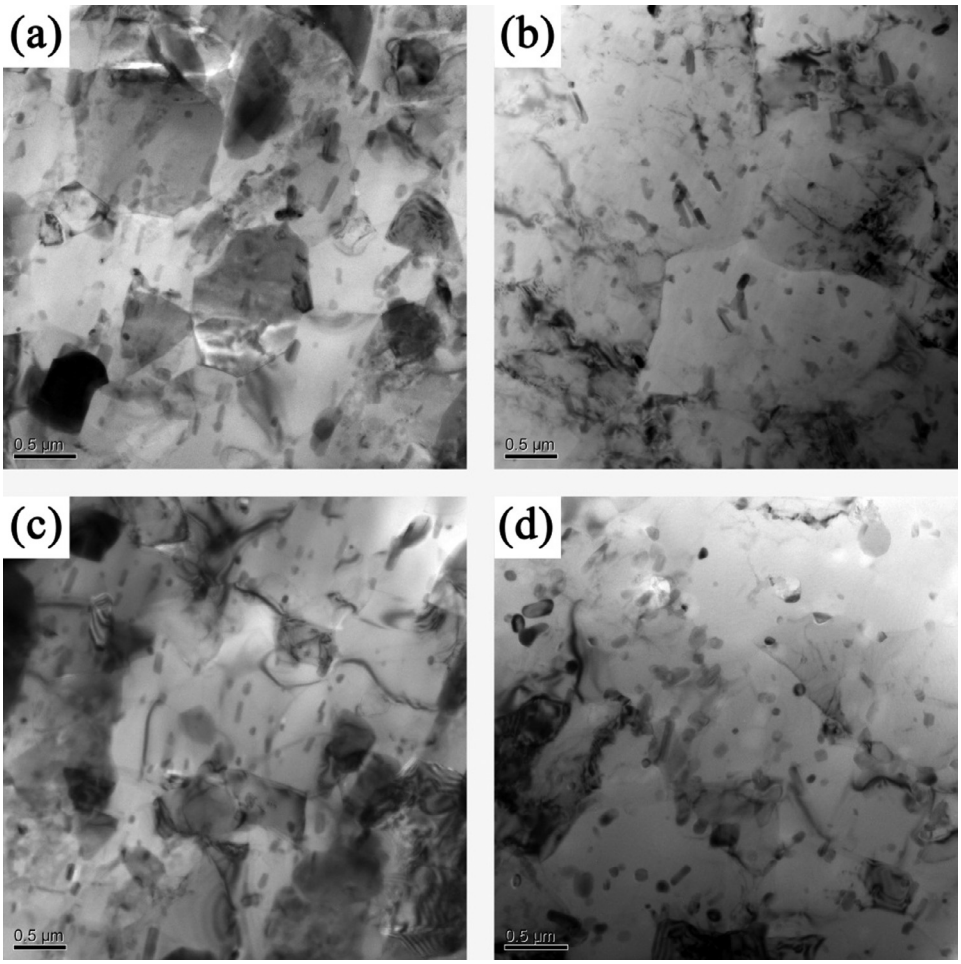

Fig. 6. TEM micrographs showing the precipitate microstructure in SZs under (a) as-welded, (b) CSed, (c) SPE and (d) HFE.

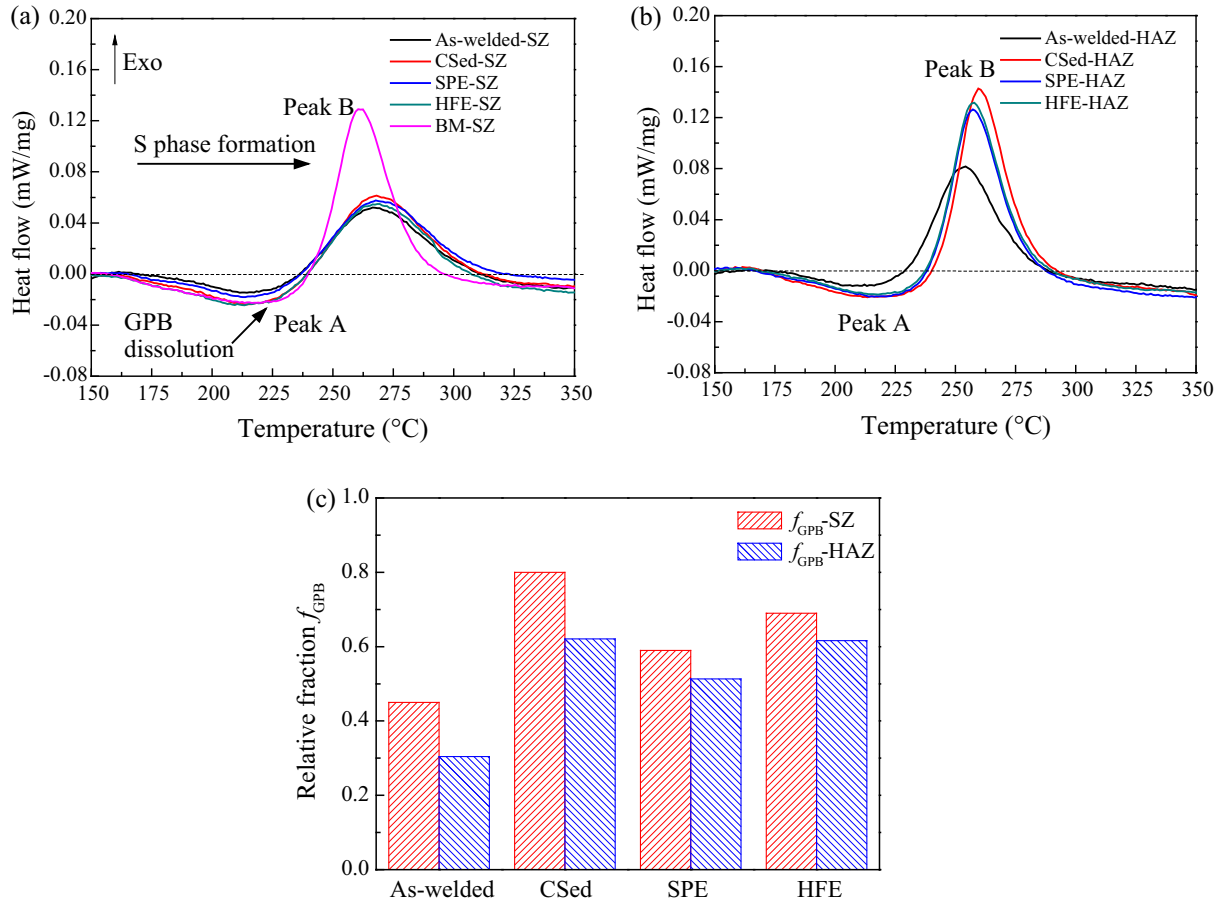

Fig. 7. DSC thermograms of the joints for (a) SZs and (b) HAZs under various cold spraying conditions; (c) relative fractions of GPB zones (f_{GPB}).

respectively. The microstructure of the FSWed AA2024-T3 joint was assumed to consist of two major phases: Guinier-Preston-Bagaryatsky (GPB) zones and S phase (Al_2CuMg). DSC curves of all specimens show a endothermic peak A around 210 °C and a exothermal peak B around 270 °C. The endotherm peak at 210 °C indicates dissolution of the GPB zones [7,47]. The peak at 270 °C is due to the precipitation of the S phase [9]. The maximum areas A and B represent the quantities of these precipitates. According to literature [7,47], area A indicates the amount of GPB present in the material, while that of B the precipitation of S phase which was transformed at the expense of GPB during the DSC measurements. It is well established that the number of GPB zones and finer S phases control hardness. Assuming a minimal coarsening of the S phase, the relative fraction of GPB zones will be by Genevois et al. [7]

$$f_{GPB} = \frac{S_A}{S_{A0}}$$

where S_A stands for the peak area A and subscript "0" denotes the BM. The calculated relative fractions of GPB zones (f_{GPB}) in SZs and HAZs are shown in Fig. 7c. For SZ specimens, the highest f_{GPB} is found for CSed, while the lowest one is for the as-welded parts. Furthermore, the f_{GPB} of the SPE is lower than that of HFE while both are between CSed and as-welded. In HAZs, the same law as SZs is followed but the f_{GPB} is lower than that in SZs. As temperature is lower in HAZ of FSW, this in effect prevents the dissolution of GPB zones, the formation and coarsening of S phase. When the joint was coated, f_{GPB} increases in both SZ and HAZ. The main reasons for these are (i) in the case of HFE, the HFE during CS could heat up the near-surface layer of the as-welded joint at a temperature between 200 and 300 °C [27,47], which improves dramatically the dissolution of the GPB zones both in SZs and HAZs; (ii) when the joint is under SPE, SPE may release residual stresses of the joints and deform grains, which may also improve the amount of the GPB zones due to a phase change induced by deformation; (iii) CS combines the effects of SPE and HFE, which increases the number of GPB zones. This explains the higher hardness values reached under different CS treatments as discussed in the next section.

3.3. Microhardness

Fig. 8 shows the microhardness profiles of the FSWed AA2024-T3 joints under various CS treatments. These hardness profiles across the joint surface layer can be classified into three groups. The hardness profiles of the as-welded and HFE are shown in Fig. 8a. The two hardness profiles have a double "W" shaped profile with two low hardness zones (LHZs) on both RS and AS sides of the joints. The hardness of the SZ and HAZ was lower than that of the BM reaching minima in the two LHZs, which were ~10 mm and 12.5 mm away from the centerline of the joint, respectively. In addition, the joint softened zone extends to 25 mm under the as-welded and HFE treatments, which size is about 2.5 times that of the tool diameter (10 mm). It can be seen that HFE affected considerably hardness and increased it throughout the whole joint, without affecting the same profile shape. Fig. 8b shows the hardness profiles of the SPE. The locations of the LHZs and the softened zone of SPE are similar to those under HFE.

Fig. 8c shows the hardness profiles of the CSed when the "HFE" and "SPE" effects were combined. It can be seen that CS increases

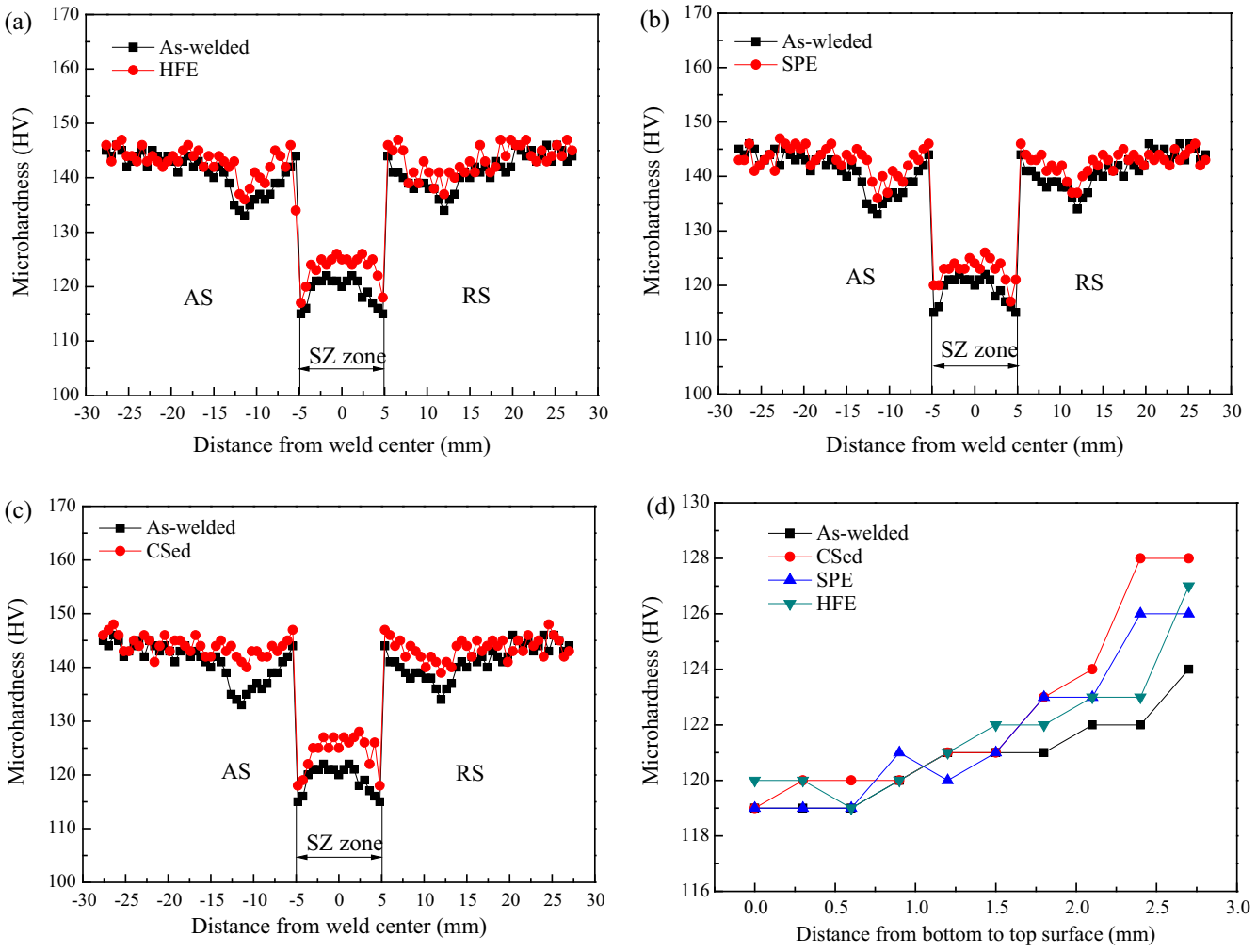

Fig. 8. Hardness profiles of FSWed AA2024-T3 joints showing effect of various CS treatments across the cross-section of the joint near the top surface: compared as-welded with (a) HFE, (b) SPE, (c) CSed and (d) along the thickness in the mid-SZ from the bottom to top surface.

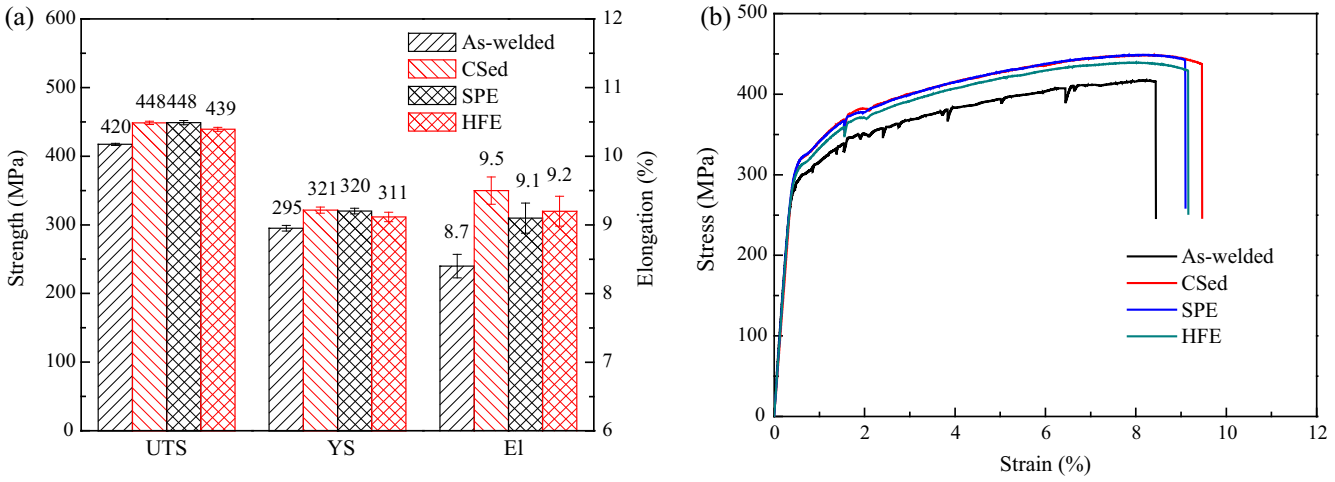

Fig. 9. Tensile test data: (a) UTS, YS and El of the joints and (b) engineering stress-strain curves.

hardness throughout the joint especially in LHZs and approached the BM level in LHZs. In addition, the hardness increase produced by CSed is larger than that of either HFE or SPE, and it is not a simple addition of the effects of the two methods. Another interesting finding is that CS makes hardness distribution more uniform on both the RS and AS sides of the joints. As shown in Fig. 8d, hardness increased almost linearly from the bottom to the top in the mid-SZ. Hardness throughout joint thickness is affected by CS as well, with

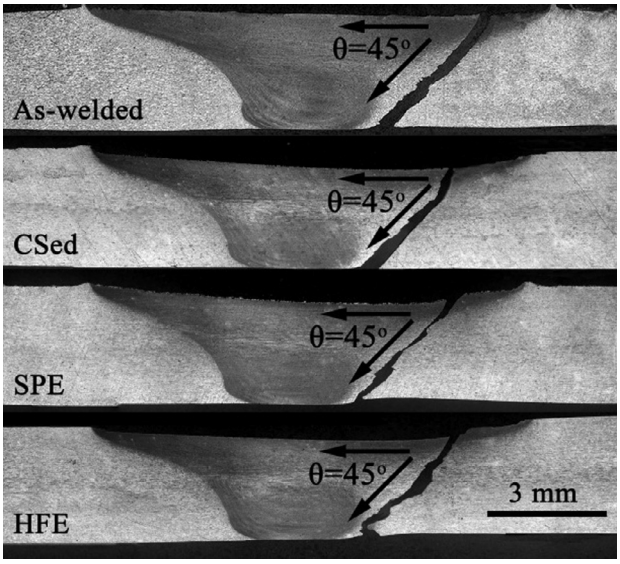

Fig. 10. Fracture locations of the joints under various cold spraying conditions.

an increase of ~7 HV at a 0.8 mm length area near the top. It is therefore safe to conclude that CSed parts have much higher hardness values than that of SPE or HFE, and the hardness value achieved is as follows: CSed > SPE ≈ HFE > as-welded.

3.4. Tensile properties and fracture location

Fig. 9a shows the ultimate strength (UTS), yield strength (YS) and elongation (El) of joints obtained under different CS treatments. The engineering stress-strain curves of BM and of individual joints are compared in Fig. 9b. Error bars in Fig. 9a indicate the total range of test results for three specimens per condition tested. It was found that the tensile properties of the joint increased from the as-welded condition by various CS treatments. The UTS and YS of the specimens tested were as follows: CSed = SPE > HFE > as-welded. The El was as follows: CSed > HFE > SPE > as-welded. The as-welded joint exhibited the lowest YS (295 MPa), UTS (420 MPa) and El (8.7%). In order to identify the tensile fracture location of the joints, the cross-sections of failed specimens were etched. The joints fractured at the SZ/HAZ interface of the RS for CS specimens, are shown in Fig. 10. Furthermore, the shear fracture path of all the joints was at a 45° angle to the tensile axis, which is the characteristic of a sound FSWed joint [9].

4. Conclusions

In this study, three CS treatments (CSed, SPE and HFE) were used to investigate the mechanism which results in improved mechanical properties. The microstructure, microhardness and tensile properties of the joints were compared and studied. The following conclusions are reached:

(1) The treatments of SPE, HFE or when CSed combined the two effects, produced a distinct improvement of microhardness and tensile properties due to microstructural change in the surface layer of the joint.
(2) A microstructural change was produced at the surface layer of the as-welded joint for the different CS treatments studied. Based on the microstructure observations, a grain refinement mechanism and improved amount of GPB zones effected by SPE, HFE or the combination of the two effects was proposed.
(3) Grains of the joints under various CS conditions become refined compared to those of the as-welded joint. The average grain sizes are about 2.3 μm, 1.9 μm, 2.0 μm and 1.9 μm for SZs obtained under as-welded, CSed, SPE and HFE conditions respectively. The dissolution of GPB zones in the SZs and HAZs did also increase with CS treatments.
(4) The effects of the HFE and SPE on the as-welded joint are not superimposed to CS but work cooperatively. All joints with CS produced superior strength-ductility results due to the higher HAGBs, refined grains, more GPB zones.

Acknowledgements

The authors would like to thank for financial support the National Natural Science Foundation of China (51574196), the 111 Project of China (B08040), the SAST of China (SAST2016043) and the National Key Research and Development Program of China (2016YFB0701203).

References

[1] M. Imam, Y. Sun, H. Fujii, N. Ma, S. Tsutsumi, H. Murakawa, Microstructural characteristics and mechanical properties of friction stir welded thick 5083 aluminum alloy, Metall. Mater. Trans. A 48 (1) (2017) 208–229.
[2] Z.H. Zhang, W.Y. Li, Y. Feng, J.L. Li, Y.J. Chao, Improving mechanical properties of friction stir welded AA2024-T3 joints by using a composite backplate, Mater. Sci. Eng. A 598 (2014) 312–318.
[3] X. Zhang, W. Yang, R. Xiao, Microstructure and mechanical properties of laser beam welded Al-Li alloy 2060 with Al-Mg filler wire, Mater. Des. 88 (2015) 446–450.
[4] J. Yan, M. Gao, G. Li, C. Zhang, X. Zeng, M. Jiang, Microstructure and mechanical properties of laser-MIG hybrid welding of 1420 Al-Li alloy, Int. J. Adv. Manuf. Tech. 66 (9–12) (2013) 1467–1473.
[5] Z.H. Zhang, W.Y. Li, J.J. Shen, Y.J. Chao, J.L. Li, Y.E. Ma, Effect of backplate diffusivity on microstructure and mechanical properties of friction stir welded joints, Mater. Des. 50 (2013) 551–557.
[6] P.L. Niu, W.Y. Li, Z.H. Zhang, X.W. Yang, Global and local constitutive behaviors of friction stir welded AA2024 joints, J. Mater. Sci, Technol, 2017.
[7] C. Genevois, A. Deschamps, A. Denquin, B. Doisneau-Cottignies, Quantitative investigation of precipitation and mechanical behaviour for AA2024 friction stir welds, Acta Mater. 53 (2005) 2447–2458.
[8] S.M. Bayazid, H. Farhangi, H. Asgharzadeh, L. Radan, A. Ghahramani, A. Mirhaji, Effect of cyclic solution treatment on microstructure and mechanical properties of friction stir welded 7075 Al alloy, Mater. Sci. Eng. A 649 (2016) 293–300.
[9] Z. Zhang, B.L. Xiao, Z.Y. Ma, Hardness recovery mechanism in the heat-affected zone during long-term natural aging and its influence on the mechanical properties and fracture behavior of friction stir welded 2024Al-T351 joints, Acta Mater. 73 (2014) 227–239.
[10] Z.H. Zhang, W.Y. Li, Y. Feng, J.L. Li, Y.J. Chao, Global anisotropic response of friction stir welded 2024 aluminum sheets, Acta Mater. 92 (2015) 117–125.
[11] Z.L. Hu, X.S. Wang, S.J. Yuan, Quantitative investigation of the tensile plastic deformation characteristic and microstructure for friction stir welded 2024 aluminum alloy, Mater. Charact. 73 (2012) 114–123.
[12] Y.M. Yue, Z.W. Li, S.D. Ji, Y.X. Huang, Z.L. Zhou, Effect of reverse-threaded pin on mechanical properties of friction stir lap welded alclad 2024 aluminum alloy, J. Mater. Sci. Technol. 32 (2016) 671–675.
[13] E. Bousquet, A. Poulon-Quintin, M. Puiggali, O. Devos, M. Touzet, Relationship between microstructure, microhardness and corrosion sensitivity of an AA 2024–T3 friction stir welded joint, Corros. Sci. 53 (2011) 3026–3034.
[14] Y. Deng, B. Peng, G.F. Xu, Q.L. Pan, R. Ye, Y.J. Wang, L.Y. Lu, Z.M. Yin, Stress corrosion cracking of a high-strength friction-stir-welded joint of an Al-Zn-Mg-Zr alloy containing 0.25 wt.% Sc, Corros. Sci. 100 (2015) 57–72.
[15] O. Hatamleh, Effects of peening on mechanical properties in friction stir welded 2195 aluminum alloy joints, Mater. Sci. Eng. A 492 (2008) 168–176.
[16] G. Liu, S.C. Wang, X.F. Lou, J. Lu, K. Lu, Low carbon steel with nanostructured surface layer induced by high-energy shot peening, Scripta Mater. 44 (2001) 1791–1795.
[17] G. İpekoğlu, G. Çam, Effects of initial temper condition and postweld heat treatment on the properties of dissimilar friction-stir-welded joints between AA7075 and AA6061 aluminum alloys, Metall. Mater. Trans. A 45 (2014) 3074–3087.
[18] C.S. Paglia, R.G. Buchheit, The influence of a propane gas torch flame post-weld heat treatment on the mechanical and corrosion properties of a 2219–T87 friction stir weld, Weld. Cut. 6 (2007) 96–102.
[19] S.J. Kalita, Microstructure and corrosion properties of diode laser melted friction stir weld of aluminum alloy 2024 T351, Appl. Surf. Sci. 257 (2011) 3985–3997.

[20] C. Padovani, A.J. Davenport, B.J. Connolly, S.W. Williams, E. Siggs, A. Groso, M. Stampanoni, Corrosion protection of AA7449-T7951 friction stir welds by laser surface melting with an excimer laser, Corros. Sci. 53 (2011) 3956–3969.
[21] C. Padovani, A.J. Davenport, B.J. Connolly, S.W. Williams, E. Siggs, A. Groso, M. Stampanoni, Corrosion protection of AA2024-T351 friction stir welds by laser surface melting with excimer laser, Corros. Eng. Sci. Technol. 47 (2012) 188–202.
[22] Y. Yang, L. Zhou, Improving corrosion resistance of friction stir welding joint of 7075 aluminum alloy by micro-arc oxidation, J. Mater. Sci. Technol. 30 (2014) 1251–1254.
[23] H.J. Liu, Y.Y. Hu, C. Dou, D.P. Sekulic, An effect of the rotation speed on microstructure and mechanical properties of the friction stir welded 2060–T8 Al-Li alloy, Mater. Charact. 123 (2017) 9–19.
[24] C.S. Paglia, K.V. Jata, R.G. Buchheit, The influence of artificial aging on the microstructure, mechanical properties, corrosion, and environmental cracking susceptibility of a 7075 friction-stir-weld, Mater. Corros. 58 (2007) 737–750.
[25] P.S. Prevey, J.T. Cammett, The influence of surface enhancement by low plasticity burnishing on the corrosion fatigue performance of AA7075-T6, Int. J. Fatigue 26 (2004) 975–982.
[26] W.Y. Li, K. Yang, S. Yin, X.W. Yang, Y.X. Xu, R. Lupoi, Solid-state additive manufacturing and repairing by cold spraying: a review, J. Mater. Sci. Technol. (2017), https://doi.org/10.1016/j.jmst.2017.09.015.
[27] W.Y. Li, S. Yin, X.P. Guo, H.L. Liao, X.F. Wang, C. Coddet, An investigation on temperature distribution within the substrate and nozzle wall in cold spraying by numerical and experimental methods, J. Therm. Spray Techn. 21 (2012) 41–48.
[28] G. Goupil, S. Jucken, D. Poirier, J.G. Legoux, E. Irissou, B. Davis, L. Roué, Cold sprayed Cu-Ni-Fe anode for Al production, Corros. Sci. 90 (2015) 259–265.
[29] R. Ghelichi, S. Bagherifard, D. MacDonald, I. Fernandez-Pariente, B. Jodoin, M. Guagliano, Experimental and numerical study of residual stress evolution in cold spray coating, Appl. Surf. Sci. 288 (2014) 26–33.
[30] S. Rech, A. Trentin, S. Vezzù, J.G. Legoux, E. Irissou, M. Guagliano, Influence of pre-heated Al 6061 substrate temperature on the residual stresses of multipass Al coatings deposited by cold spray, J. Therm. Spray Techn. 20 (2011) 243–251.
[31] W.Y. Li, R.R. Jiang, C.J. Huang, Z.H. Zhang, Y. Feng, Effect of cold sprayed Al coating on mechanical property and corrosion behavior of friction stir welded AA2024-T351 joint, Mater. Des. 65 (2015) 757–761.
[32] W.Y. Li, N. Li, X.W. Yang, Y. Feng, A. Vairis, Impact of cold spraying on microstructure and mechanical properties of optimized friction stir welded AA2024-T3 joint, Mater. Sci. Eng. A 702 (2017) 73–80.
[33] F.S.D. Silva, J. Bedoya, S. Dosta, N. Cinca, I.G. Cano, J.M. Guilemany, A.V. Benedetti, Corrosion characteristics of cold gas spray coatings of reinforced aluminum deposited onto carbon steel, Corros. Sci. 114 (2017) 57–71.
[34] H. Assadi, H. Kreye, F. Gärtner, T. Klassen, Cold spraying-a materials perspective, Acta Mater. 116 (2016) 382–407.
[35] R.M. Souto, M.M. Laz, R.L. Reis, Degradation characteristics of hydroxyapatite coatings on orthopaedic TiAlV in simulated physiological media investigated by electrochemical impedance spectroscopy, Biomaterials 24 (2003) 4213–4221.
[36] X. Zhou, P. Mohanty, Corrosion behavior of cold sprayed titanium coatings in simulated body fluid, Corros. Eng. Sci. Technol. 47 (2012) 145–154.
[37] C. Hamilton, S. Dymek, M. Blicharski, A model of material flow during friction stir welding, Mater. Charact. 59 (2008) 1206–1214.
[38] M.R. Rokni, C.A. Widener, V.K. Champagne, S.R. Nutt, The effects of heat treatment on 7075 Al cold spray deposits, Surf. Coat. Technol. 310 (2016) 278–285.
[39] S. Yin, X.F. Wang, X.K. Suo, H.L. Liao, Z.W. Guo, W.Y. Li, C. Coddet, Deposition behavior of thermally softened copper particles in cold spraying, Acta Mater. 61 (2013) 5105–5118.
[40] V. Luzin, K. Spencer, M.X. Zhang, Residual stress and thermo-mechanical properties of cold spray metal coatings, Acta Mater. 59 (2011) 1259–1270.
[41] X. Wu, N. Tao, Y. Hong, B. Xu, J. Lu, K. Lu, Microstructure and evolution of mechanically-induced ultrafine grain in surface layer of AL-alloy subjected to USSP, Acta Mater. 50 (2002) 2075–2084.
[42] X.C. Liu, H.W. Zhang, K. Lu, Strain-induced ultrahard and ultrastable nanolaminated structure in nickel, Sci. 342 (2013) 337–340.
[43] L. Lu, Y. Shen, X. Chen, L. Qian, K. Lu, Ultrahigh strength and high electrical conductivity in copper, Science 304 (2004) 422–426.
[44] S.C. Wang, M.J. Starink, Precipitates and intermetallic phases in precipitation hardening Al-Cu-Mg-(Li) based alloys, Int. Mater. Rev. 50 (2005) 193–215.
[45] Y.H. Zhao, Y.T. Zhu, E.J. Lavernia, Preparation of nanostructured materials having improved ductility, Adv. Eng. Mater. 12 (2010) 769–788.
[46] M.J. Starink, Analysis of aluminium based alloys by calorimetry: quantitative analysis of reactions and reaction kinetics, Int. Mater. Rev. 49 (2004) 191–226.
[47] V. Dixit, R.S. Mishra, R.J. Lederich, R. Talwar, Influence of process parameters on microstructural evolution and mechanical properties in friction stirred Al-2024 (T3) alloy, Sci. Technol. Weld. Join. 14 (2009) 346–355.